

Classification of Breast Tumours Based on Histopathology Images Using Deep Features and Ensemble of Gradient Boosting Methods

Mohammad Reza Abbasniya¹, Sayed Ali Sheikholeslamzadeh¹, Hamid Nasiri^{2,*} and Samaneh Emami¹

^aDepartment of Electrical and Computer Engineering, Semnan University, Semnan, Iran

^bDepartment of Computer Engineering, Amirkabir University of Technology, Tehran, Iran

ARTICLE INFO

Keywords:

BreakHis
Breast Cancer
Ensemble classification
Grad-CAM
Inception-ResNet-v2
Transfer learning

ABSTRACT

Breast cancer is the most common cancer among women worldwide. Early-stage diagnosis of breast cancer can significantly improve the efficiency of treatment. Computer-aided diagnosis (CAD) systems are widely adopted in this issue due to their reliability, accuracy and affordability. There are different imaging techniques for a breast cancer diagnosis; one of the most accurate ones is histopathology which is used in this paper. Deep feature transfer learning is used as the main idea of the proposed CAD system's feature extractor. Although 16 different pre-trained networks have been tested in this study, our main focus is on the classification phase. The Inception-ResNet-v2 which has both residual and inception networks profits together has shown the best feature extraction capability in the case of breast cancer histopathology images among all tested CNNs. In the classification phase, the ensemble of CatBoost, XGBoost and LightGBM has provided the best average accuracy. The BreakHis dataset was used to evaluate the proposed method. BreakHis contains 7909 histopathology images (2,480 benign and 5,429 malignant) in four magnification factors. The proposed method's accuracy (IRv2-CXL) using 70% of BreakHis dataset as training data in 40x, 100x, 200x and 400x magnification is 96.82%, 95.84%, 97.01% and 96.15%, respectively. Most studies on automated breast cancer detection have focused on feature extraction, which made us attend to the classification phase. IRv2-CXL has shown better or comparable results in all magnifications due to using the soft voting ensemble method which could combine the advantages of CatBoost, XGBoost and LightGBM together.

1. Introduction

The term cancer is a generic word for an extensive group of diseases which may affect different parts of the body. To understand cancer, we must first know about Tumours. Tumours can either be benign or malignant which are recognized as cancerous. Tumours that are deemed to be benign (noncancerous) increase in size slowly and do not spread. Cancerous tumours grow swiftly, overrun and dismantle nearby healthy tissues throughout the whole body [1]. Breast cancer arises in lining cells of ducts or lobules in the glandular tissue of the breast [2]. According to the WHO, breast cancer is the most prevalent cancer worldwide and the fifth most common cause of cancer death in 2020². If breast cancer is detected at its early stages, it can be treated quite effectively before it spreads to other parts of the body [3].

Breast cancer is diagnosed using various imaging techniques such as mammography, ultrasound, thermography and pathological tests [4, 5]. Among these methods, for those patients who have undergone other forms of scannings, histopathology images are considered to be the gold standard for improving the accuracy of results as well as providing reliable information for assessing the effects of cancer on surrounding tissue [5]. Histopathological images of tissues from breast tumour patients are obtained by applying certain chemicals

to dye the nucleus of the cells and then dyeing the other components with another chemical in different shades to accentuate various parts tissue structures and cellular characteristics [5].

After completing the biopsy, diagnosis will be done by a pathologist who will examine the stained tissue using a microscope. Although these images are very comprehensive, due to various difficulties such as scant contrast in images, noise and lack of appreciation by the human eye the occurrence of misdiagnoses are fairly possible [6]. Add to this a lack of well-trained specialists and the extremely time-consuming analysis of H&E-stained images using microscopes and it becomes understandable why an alternative method to using human specialists is needed [7]. With the onset of pattern recognition, machine learning (ML) and convolutional neural networks, to overcome existing problems, researchers are focusing on using CAD to improve tests accuracy [5]. CAD systems are classified into two different categories. One category sorts the systems by the staining method of images used as input, which are H&E-stained and IHC images. Images obtained by using haematoxylin and eosin are more suited for determining whether a neoplasm is cancerous or not but analysis of these images calls for more sophisticated image processing and machine learning methods. Immunohistochemistry images which are marked by certain biomarkers to illustrate certain cells or regions are especially handy when cancer has already been diagnosed using the H&E method. [8].

Another method for categorizing CAD systems is grouping them by whether the images they use are WSI or ROI.

*Correspondence should be addressed to Hamid Nasiri; h.nasiri@aut.ac.ir

¹These authors contributed equally to this work and should be regarded as co-first authors.

²<https://www.who.int/news-room/fact-sheets/detail/cancer>, Retrieved on 2022-2-20

Both H&E-stained and IHC images are used as input in these systems. For diagnosis using WSI as input, the entirety of images is used without any tampering. In systems that use ROI however key parts are concentrated on using segmentation or image detection [8]. In analysing WSI's, no segmentation or path determination are done on images with the goal of the system recognizing cancerous and noncancerous slides. With this fact in mind experts are only required to label the images in the training phase as either benign or malignant [8]. CAD systems use different algorithms and structures for tumour classification; this study aims to propose a new method for binary classification of tumours based on histopathology whole slide images using deep feature transfer learning.

Transfer learning is a deep learning method where one models knowledge is passed on to another model [9]. Using transfer learning algorithms reduces training time of models drastically, allowing for different solutions to be built straight away. Furthermore, it can save us from establishing an expensive and complicated cloud GPU/TPU. One other noteworthy benefit of using transfer learning reveals itself in tackling a lack of data. For deep learning models to solve a task successfully, a good deal of data is needed. However, cases, where data is abundantly available, are few and far between, leaving us to deal with a lack of data most of the time, as evident in the case of breast tumour classification [10, 11].

2. Related Works

An early-stage breast cancer diagnosis can substantially decrease its mortality rate; as such, CAD systems using ML approaches could be widely effective here. As any other ML problem, researchers and data scientists need enough data to be involved in this context. Therefore, many different datasets have been provided with various imaging modalities such as Mammograms (MGs), Ultrasound (US), Magnetic Resonance Imaging (MRI) and Histopathology (HP) [12].

For example, the Bioimaging dataset containing 156 annotated H&E-stained images in size 2048×1536 divided into four classes (normal, benign, in situ and invasive) is used in a study by Fondon et al. (2018) [13]. In their work, contrast level adaptive histogram equalization is used for preprocessing images and in the next step 250 numerical features based on nuclei, colour region and texture characteristics are extracted, and finally, an SVM classifier is adopted to classify images according to extracted features.

In another study by George et al. (2020) [14], 200 \times magnification images of the BreakHis [15] dataset was used to evaluate their method. The NucTraL+BCF is their suggested method which consists of four sections; first the Macenko [16] strategy is used for stain normalization as the preprocessing phase, then nucleus paths are extracted from images and enter into three individual transfer learning-based processes. Each process utilizes an SVM classifier and in the final section, belief theoretical classifier fusion is used

to determine the final result according to results provided by three SVM classifiers.

In addition, invasive ductal carcinoma (IDC) is an imbalanced dataset that contains 277,524 colour images divided into two classes (negative and positive). This dataset is used by Choudhary et al. (2021) [17]. In their study, several CNNs and the pruned version of them were employed to train on 70% of the dataset's images by two strategies, training the whole CNN or only the last layer. The pruned version of ResNet50, in which all layers were trained, has shown the best performance in that case. Another study by Barsha et al. (2021) [18] tried to use an ensemble of two pre-trained CNNs on the same dataset (IDC), but the training size was 80% of the dataset. In that paper, a dense layer with softmax activation was added to the end of the DenseNet-121 and DenseNet-169 networks for binary classification. Test time augmentation was employed to increase model accuracy and the final decision was reached by using the mean of prediction probabilities.

Thermography infrared is another technique for medical imaging which can be used in the breast cancer diagnosis process. This technique is used in collecting DMR-IR dataset which is adopted widely to evaluate state-of-the-art breast cancer diagnosis methods such as the proposed methods by Gonçalves et al. (2022) [19] and Chatterjee et al. (2022) [20]. Similar to other mentioned works, Gonçalves et al. also used pre-trained CNNs. They utilized original weighted networks of VGG-16, ResNet-50 and DenseNet-201 and then tried to search for the best architecture of the fully connected layer to be adopted as a binary classifier at the end of each CNN. In that paper, two bio-inspired algorithms (i.e., Genetic Algorithm and Particle swarm optimization) were suggested as searching methods. In the study by Chatterjee et al. [20] pre-trained version of VGG-16 was used to extract image features as well. The distinctive point of their study is to use a memory-optimized version of the Dragonfly Algorithm to reduce the dimension of the features vector by about 40% before adopting an SVM classifier.

3. Materials and Methodology

3.1. Dataset

In this article Breast Cancer Histopathological Image Classification (BreakHis) dataset is used in order to examine the viability of our method [15]. The BreakHis dataset was collected in a clinical study by Pathological Anatomy and Cytopathology Laboratory, Parana state, Brazil from January to December of 2014. BreakHis is a public and well-known dataset that contains 7,909 high-quality images taken from the microscopic biopsy of benign and malignant (2,480 and 5,429 images respectively) breast tumours. BreakHis dataset contains two procedures of biopsy: Surgical Open Biopsy (SOB) and Core Needle Biopsy (CNB) section of $\sim 3\mu\text{m}$ thickness. In addition, haematoxylin and eosin (HE) stained breast tissue biopsy slides are used in the process of collecting images. Image acquisition is done by Olympus BX-50 microscope with a 3.3 \times magnification relay lens coupled to

SCC-131AN which is a Samsung digital colour camera with 6.5 μm pixel size. These images were collected from 82 patients at four magnifying factors: 40 \times , 100 \times , 200 \times and 400 \times . In fact, these magnifications are produced by 4 \times , 10 \times , 20 \times , and 40 \times objective lens, respectively and a 10 \times ocular lens. No normalization nor colour standardization was undertaken on the raw images. Each image is in 700 \times 460 pixels dimension with a 3-byte colour depth (3-channels: Red, Green, Blue) and saved in Portable Network Graphics (PNG) format. The BreakHis dataset determines the class of tumours (Benign or Malignant) as well as their type. There are four types of each tumour class. Benign tumour types: Adenosis, Fibroadenoma, Tubular Adenoma and Phyllodes Tumour; Malignant tumour types: Ductal Carcinoma, Lobular Carcinoma, Mucinous Carcinoma (Colloid) and Papillary Carcinoma [15]. Some samples of these tumour types are shown in Figure 1 with the magnification specific class distribution in Table 1. For this research we used 70% of the images in the dataset as training set and the remaining 30% as test set.

Table 1
Distribution of BreakHis samples.

BreakHis Magnification factor	Benign	Malignant	Total
40 \times	652	1370	1995
100 \times	644	1437	2081
200 \times	623	1390	2013
400 \times	588	5429	1820
Total	2480	5429	7909

Since BreakHis uses the Histopathology (HP) method which provides coloured images and the possibility of in-depth tissue analysis, there is more chance for early-stage diagnosis of cancer and higher confidence on the results in comparison with other methods. this method is known as an invasive method and requires high care in the process of biopsy [12].

3.2. Methodology

Transfer learning is the main idea for the proposed model's binary classification on the BreakHis dataset. Stevo Bozinski and Ante Fulgosi were the first to mention using transfer learning in a neural network [21]. Their paper was published in 1976, five years later they reported the transfer learning application in training a neural network on a dataset of computer terminal letter images.

Deep feature transfer learning is the idea of using a neural network that is trained on a massive dataset such as ImageNet [22] with hundreds of classes to predict labels on another dataset. This idea could be achieved by removing fully connected layers, which are used to classify images according to features extracted by convolutional layers and adding another classifier to the network, therefore allowing us to use features extracted by a network with a massive dataset with

another classification method in different models. The classifier we add to the model can either be a fully connected layer or one based on other classification algorithms.

3.2.1. Feature Extractor

After testing 16 pre-trained neural networks, Inception-ResNet-v2 which is trained on ImageNet showed the most promising results in our case; Accuracies of extracting features by different neural networks are available in section 4. The Inception-ResNet-v2 was first introduced by Szegedy et al. in 2016 [23]. The idea of this neural network consists of residual connections and architecture of Inception. To achieve the advantages of residual connection and its efficiency in computation at the same time, the filter connection stage of Inception architecture was replaced with residual connections. In [23], the authors argued that using residual connections causes great improvement in training speed. The architecture of Inception-ResNet-v2 is illustrated in Figure 4. Every convolution marked by "V" is a valid-padded layer (filter window stays inside the input) and those that are not marked by "V" are same-padded (output window is the same size as the input). There are three inception blocks in the architecture of Inception-ResNet-v2 and in each block, just before matching the depth of input, a 1 \times 1 convolution layer is placed to increase the filter bank dimensionality [23].

3.2.2. Gradient Class Activation Map (Grad-CAM)

Spatial information is naturally preserved in convolutional layers in general and as a result, it is anticipated that the last convolutional layer of the feature extractor has the best balance between high-level semantics and detailed spatial information. Neurons in the last convolutional layer search for semantic class-specific data in the given image [24]. Gradient information streaming into these layers is used by Grad-CAM to appoint significance values to each neuron for a specific decision of interest, thus emphasizing the identification area for each class in the input image [24, 25]. In other words, Grad-CAM determines the gradient of a particular class grade with regards to the pixel of the feature map and then averages gradients of each channel to come by channel-wise weight [26]. With this information, it is possible for us to disclose the internal logic of CNNs as well as provide clinical references about patients' data and health status to a greater extent [27, 28, 29]. We can also regard these visual insights to determine where the model is failing and why then address these problems by changing the model's architecture [30]. Examples of applying grad-cam on features extracted by Inception-ResNet-v2 are shown in Table 2.

3.2.3. Classifier

Three different classifiers were used in a variety of different model structures in this study to determine whether a tumour is benign or malignant based on the deep features extracted by the deep neural network, however, we will only discuss the model that lent to the best results and only mention the others. XGBoost, CatBoost and LightGBM were used alone in three of the seven models while the other four

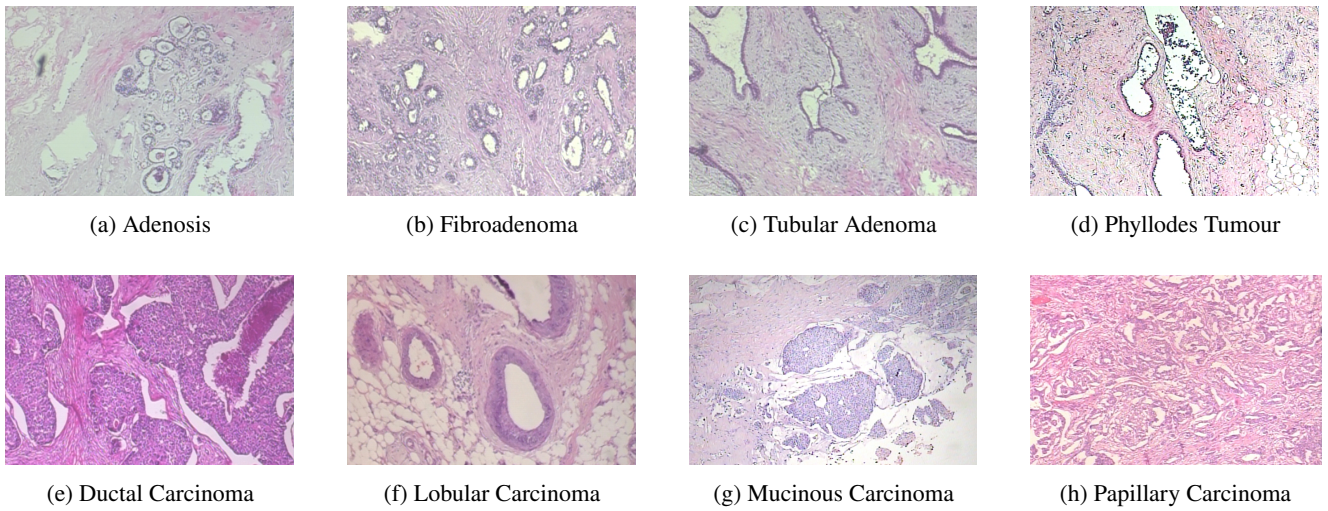


Figure 1: Samples of benign (a-d) and malignant (e-h) tumour types in 40× magnification.

Table 2
Inception-ResNet-v2 Grad-CAM visualization samples.

Tumour class	Original biopsy image	Heatmap	Grad-CAM
Benign			
Malignant			

used a soft voting ensemble method of two or all three of the mentioned classifiers instead. Best results were achieved by LightGBM, XGBoost and CatBoost classifier's soft voting which is described in 3.2.4.

LightGBM: Gradient boosting decision tree (GBDT) is a time-honoured model that utilizes a weak classifier, namely a decision tree, with iterative training to achieve a top-notch model that enjoys such advantages as competent training effect and resistance to overfitting [31]. LightGBM (light gradient boosting machine) is a speedy, open-source lifting frame-

work based on GBDT which has a faster training speed, lower memory consumption, and better accuracy [32, 33]. LightGBM can quickly process massive data by instigating leaf-wise tree growth (see Figure 2) with depth limitation and gradient-based one-side sampling as well as exclusive feature bundling approaches [31, 34]. LightGBM hyperparameters were tuned by trial and error.

CatBoost: This algorithm integrates GBDT and categorical features hence the name CatBoost. CatBoost is oblivious tree-based with fewer parameters and categorical variable support. The mentioned implementation also handles gradient bias and prediction shift, doing so improves the generalization and robustness of the algorithm [35]. CatBoost (categorical boosting) uses permutation, target-based statistics and one-hot-max-size (OHMS) to emphasize categorical columns while utilizing the greedy algorithm at each new tree split to resolve the exponential feature combination increase [36]. CatBoost boasts the characteristics of high classification accuracy and fast training speed [37]. In fact, the highest single magnification classification accuracy result (i.e., 97.49%) was achieved by using CatBoost as the model's classifier however the ensemble method worked better across all magnifications in average. In this study, CatBoost hyperparameters were tuned by trial and error.

XGBoost: Extreme Gradient Boosting (XGBoost) [38], like the other two classifiers used in the proposed majority voting ensemble method, is a technique that uses the results of several decision trees to generate a prediction score [39]. This method expands the tree level-wise (see Figure 3) by constantly dividing features. Every tree then computes the feature and threshold with the best branch effect and proceeds to complete the split. Simply put, XGBoost yields better results than conventional decision trees by utilizing classification and regression trees as base learners to consecutively blend various tree predictions with the use of gradient boosting as an error minimizer [28]. XGBoost also lowers the likelihood of over-fitting through regularization by employing a second-order Taylor series to approximate the value of the loss function [39, 40, 41]. All of this makes XGBoost a gradient boosting library optimized for efficiency, versatility and portability [42, 43]. XGBoost hyperparameters were tuned by trial and error.

3.2.4. Ensemble Classification

In this study, three fine-tuned classifiers are used to predict the probability of malignancy based on features vector obtained from pre-trained CNNs. We decided to implement different combinations of these classifiers, which use a form of ensemble learning themselves, by utilizing another ensemble method. There are multiple ways to adopt ensemble learning in classification, but here we use one of the most common ones called Soft-Voting. In this approach, every classifier produces a probability for each class, the mean of which is considered as the final probability of that class [44]. Finally, the class with the highest probability will be the agreement of ensembled classifiers. This approach has no

limitation on the number of classifiers while another method like Majority-Voting can only ensemble an even number of classifiers.



Figure 2: LightGBM leaf-wise tree growth.

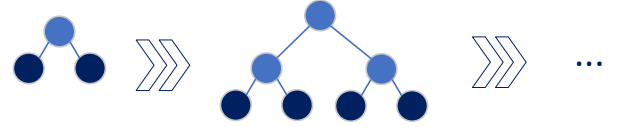


Figure 3: XGBoost level-wise tree growth.

4. Result and Discussion

4.1. Evaluation Metrics

In our binary classification of the BreakHis dataset, predicted labels can be split into four different categories by comparing them to actual labels of test set: TP (number of correct malignant predictions), TN (number of correct benign predictions), FP (number of incorrect malignant predictions), FN (number of incorrect benign predictions). The following are different evaluation metrics used in this paper:

$$Accuracy = \frac{TP + TN}{TP + FP + TN + FN} \quad (1)$$

$$Balanced\ accuracy = \frac{1}{2} \left(\frac{TP}{TP + FN} + \frac{TN}{TN + FP} \right) \quad (2)$$

$$F_1\ score = \frac{TP}{TP + \frac{1}{2}(FP + FN)} \quad (3)$$

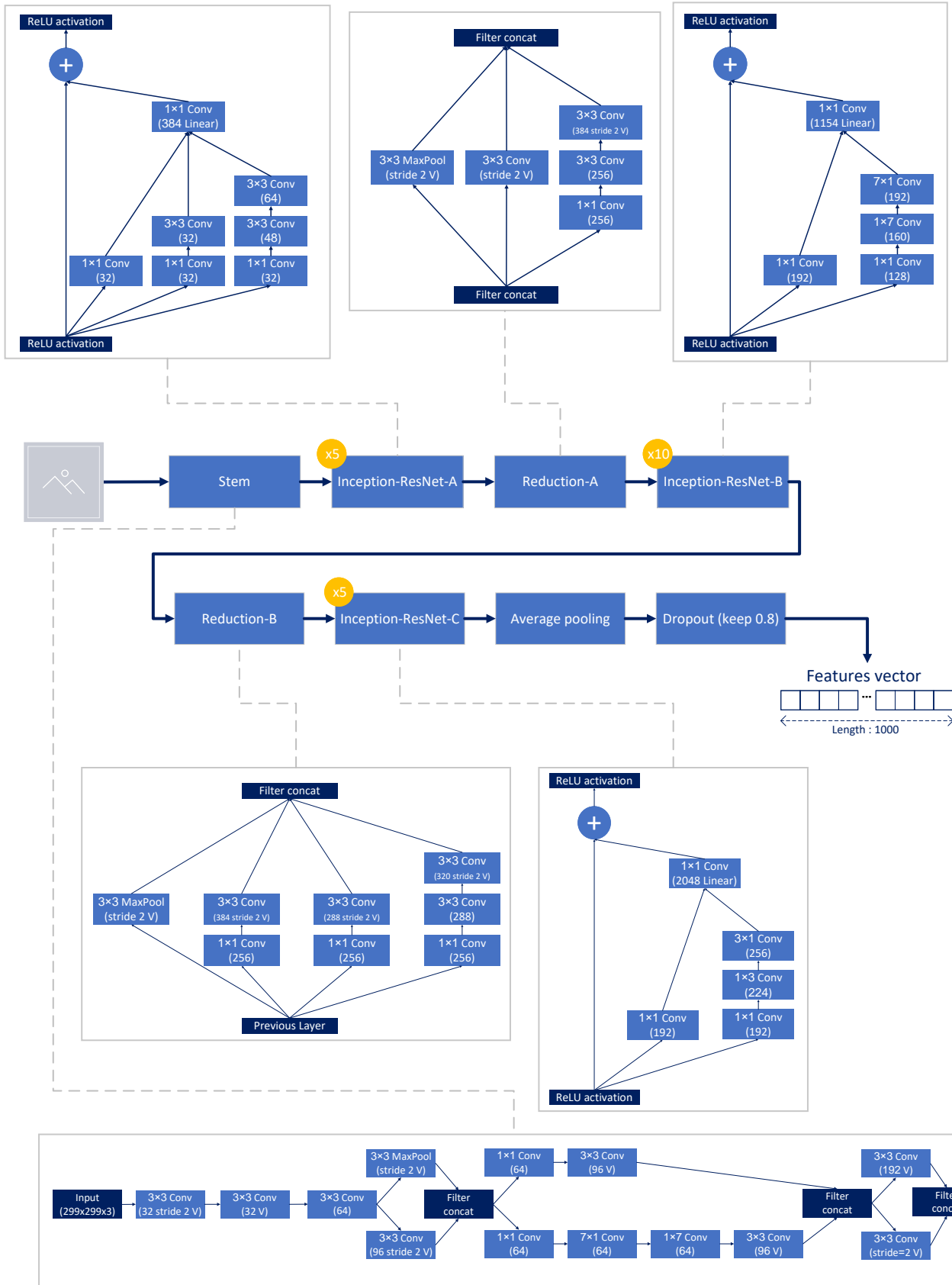


Figure 4: Architecture of Inception-ResNet-v2 as feature extractor.

4.2. Binary Classification Results

In this paper, 16 pre-trained networks were used to extract features from input images. Features were then supplied to seven different classifiers (three single and four soft voting ensembles) to predict our final labels. Results of the performance of individual and ensemble models on the test set are available in Table 4; X, L and C stand for XGBoost, LightGBM and CatBoost, respectively. The Keras implementation of the pre-trained networks (CNN) is used in this research. For each network, a simple preprocessing method recommended by Keras is used before feeding images to the CNNs³. The Google-Colaboratory free environment (12GB RAM, 78GB disk and cloud GPU) has been used for models implementation.

4.3. Proposed Method

As evident by the results presented in Table 4, the combination of Inception-ResNet-v2 as feature extractor and an ensemble of all three classifiers produced the best accuracy among all 112 tested models (results with the f1-score as an evaluation metric are also available in Table 5), so it was selected as the proposed method of this study. It consists of Inception-ResNet-v2 and ensemble of CatBoost, XGBoost, and LightGBM, which we named IRv2-CXL. The full architecture of IRv2-CXL is illustrated in Figure 5. By reviewing Benhammou [45] and the other studies mentioned in related works, we concluded that ResNet50, DensNet201 and Inception-v3 networks are three of the more commonly used pre-trained networks in breast tumours classification. Therefore, we decided to compare the ROC curve of these networks with Inception-ResNet-v2 using the chosen classifier (i.e., CXL). Results are shown in Figure 6. Other evaluation metrics applied to the proposed method are provided in Table 3 and the magnification specific confusion matrix in Figure 7.

Table 3
Proposed method (IRv2-CXL) evaluation.

Metric	Results				Average
	40×	100×	200×	400×	
Accuracy	96.83%	95.84%	97.01%	96.15%	96.46%
Balanced accuracy	95.64%	94.90%	95.89%	95.15%	95.40%
F ₁ score	97.76%	97.03%	97.87%	97.11%	97.44%

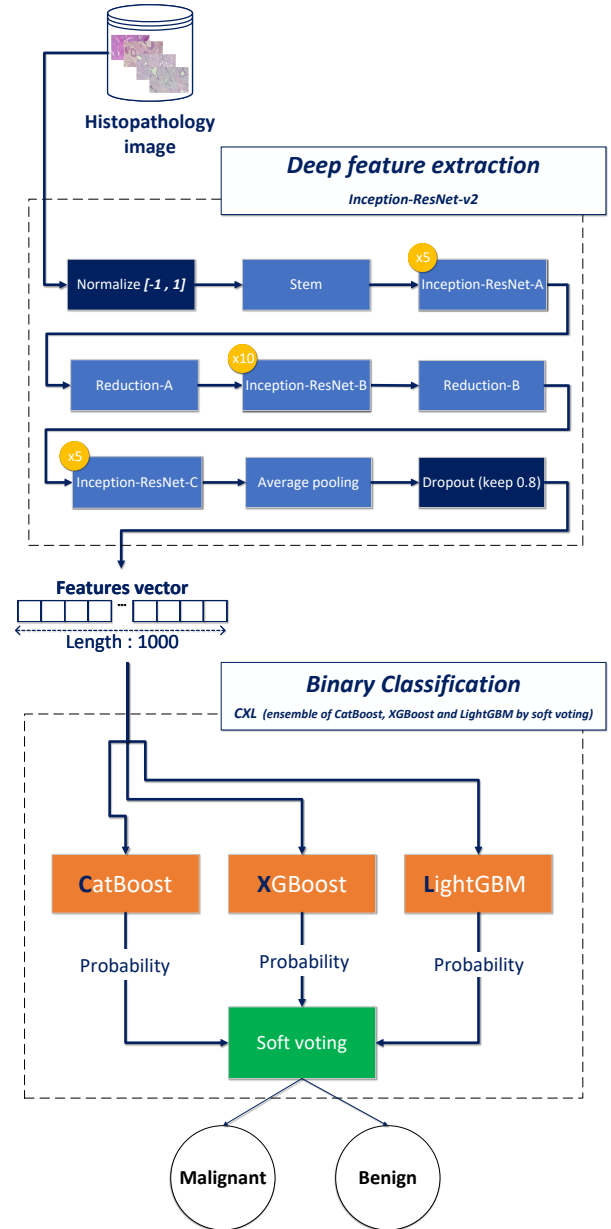
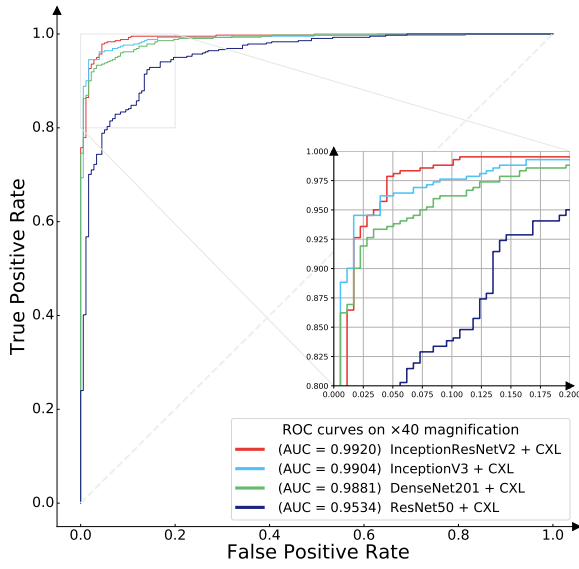


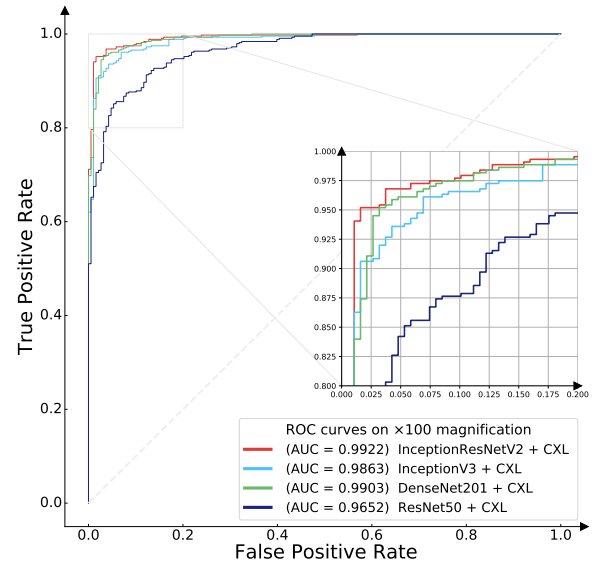
Figure 5: Proposed method (IRv2-CXL) architecture.

³<https://github.com/keras-team/keras/tree/master/keras/applications>, Retrieved on 2021-8-5

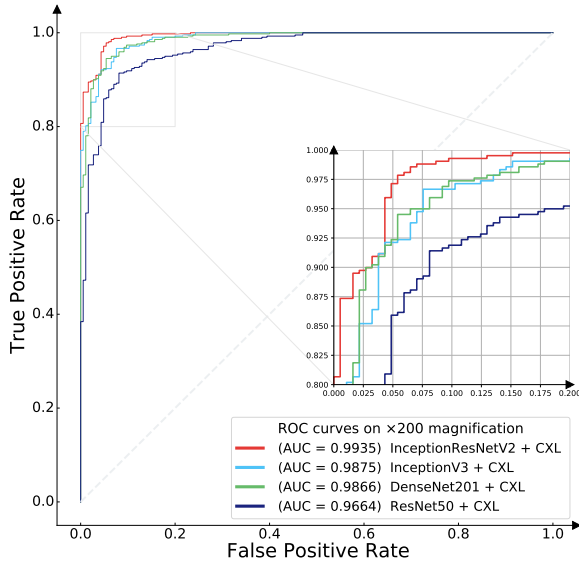
Classification of Breast Tumours Using Gradient Boosting Methods



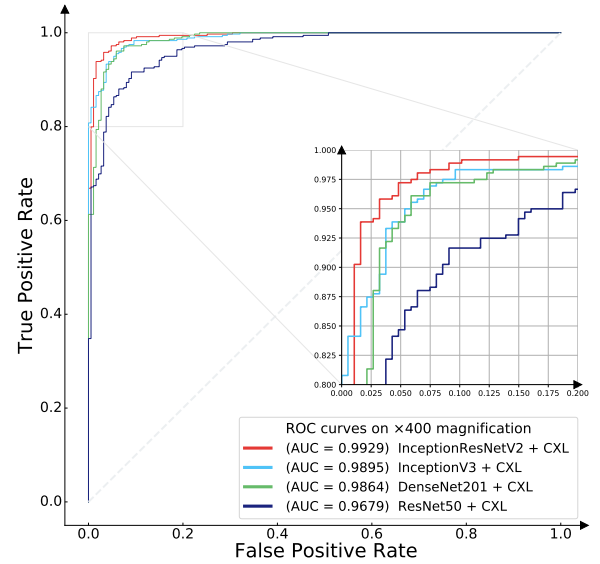
(a)



(b)



(c)



(d)

Figure 6: ROC curves of different feature extractors classified by CXL. (a) $40\times$, (b) $100\times$, (c) $200\times$, (d) $400\times$.

		Actual	
		Malignant +	Benign -
Prediction	Malignant +	415	6
	Benign -	13	165

(a)

		Actual	
		Malignant +	Benign -
Prediction	Malignant +	425	12
	Benign -	14	174

(b)

		Actual	
		Malignant +	Benign -
Prediction	Malignant +	414	5
	Benign -	13	172

(c)

		Actual	
		Malignant +	Benign -
Prediction	Malignant +	353	6
	Benign -	15	172

(d)

Figure 7: IRv2-CXL confusion matrix on different test set magnifications. (a) $40\times$, (b) $100\times$, (c) $200\times$, (d) $400\times$.

Table 4Binary classification **accuracy** results on BreakHis dataset.

Feature extractor	Classifier(s)	Result (accuracy %)				Feature extractor	Classifier(s)	Result (accuracy %)			
		40×	100×	200×	400×			40×	100×	200×	400×
VGG 16	X	85.64	81.44	83.44	78.20	Inception v3	X	94.49	93.6	94.7	93.58
	L	85.97	82.56	85.26	78.38		L	95.82	94.56	94.53	94.68
	C	86.47	83.68	85.59	78.93		C	95.15	93.44	93.70	94.13
	X & L	87.31	82.88	84.76	79.48		X & L	94.99	93.92	94.86	95.23
	X & C	86.64	82.24	84.76	79.30		X & C	95.15	93.76	94.70	94.87
	L & C	86.31	84.00	85.09	79.48		L & C	95.32	94.08	94.70	94.87
	X & L & C	86.97	83.04	84.76	78.93		X & L & C	95.49	94.24	94.53	95.23
VGG 19	X	85.64	80.32	83.27	78.38	Inception ResNet v2	X	96.32	95.36	95.36	95.97
	L	84.47	83.04	83.6	78.20		L	96.82	95.52	96.85	96.33
	C	85.97	82.72	85.43	79.67		C	97.49	95.84	96.19	95.97
	X & L	85.64	81.6	85.43	80.58		X & L	96.49	95.84	96.68	96.52
	X & C	86.81	81.92	85.59	80.4		X & C	96.82	96.16	96.35	95.78
	L & C	85.14	82.56	84.60	79.67		L & C	96.99	96.16	96.68	95.42
	X & L & C	85.80	82.40	85.92	80.03		X & L & C	96.82	95.84	97.01	96.15
ResNet 50	X	87.81	89.6	90.39	90.65	DenseNet 121	X	93.99	95.2	93.54	95.23
	L	89.81	89.92	90.72	90.10		L	94.15	95.84	94.53	95.23
	C	89.14	90.08	91.05	89.92		C	94.15	94.72	93.87	94.50
	X & L	89.81	90.56	91.05	90.29		X & L	94.65	96.16	94.37	94.87
	X & C	89.31	90.56	91.39	90.29		X & C	93.99	95.20	94.03	94.87
	L & C	90.15	90.08	90.89	90.84		L & C	93.99	95.36	94.37	95.42
	X & L & C	89.48	90.72	91.22	90.84		X & L & C	94.65	95.20	95.03	95.23
ResNet 101	X	86.14	86.4	87.58	87.36	DenseNet 169	X	94.65	96.00	94.20	94.68
	L	86.47	88.16	89.4	88.09		L	94.65	96.64	94.20	93.77
	C	87.14	88.00	90.06	89.56		C	93.15	96.16	94.86	94.50
	X & L	86.14	87.68	88.90	87.72		X & L	94.65	95.84	94.20	94.13
	X & C	86.97	88.00	89.56	88.46		X & C	93.99	95.68	94.20	94.68
	L & C	87.31	88.64	89.73	88.82		L & C	94.15	96.48	94.70	93.95
	X & L & C	86.64	88.32	89.56	88.46		X & L & C	94.32	96.00	94.70	93.95
ResNet 152	X	86.14	84.96	88.57	86.26	DenseNet 201	X	92.98	95.2	93.37	95.23
	L	86.14	85.92	88.57	86.63		L	93.99	95.36	95.03	94.87
	C	86.14	87.04	88.74	85.34		C	93.82	95.36	94.53	93.58
	X & L	86.47	85.76	89.56	86.26		X & L	94.49	95.04	94.70	95.05
	X & C	86.97	86.24	88.90	86.81		X & C	93.65	94.88	94.20	94.68
	L & C	86.31	85.92	89.40	86.44		L & C	94.15	95.68	94.86	94.32
	X & L & C	86.47	85.92	89.07	87.17		X & L & C	94.32	95.52	95.03	94.50
ResNet 50-v2	X	95.49	94.24	93.54	92.67	Xception	X	92.15	91.04	92.88	92.85
	L	94.65	95.52	94.20	94.13		L	93.65	92.16	92.05	94.13
	C	94.65	95.52	93.70	93.04		C	90.98	92.00	91.72	90.47
	X & L	95.82	95.84	94.37	93.77		X & L	93.65	92.32	93.04	93.4
	X & C	95.82	95.04	94.03	92.67		X & C	92.48	92.32	91.72	92.12
	L & C	94.99	95.68	94.53	93.40		L & C	92.98	92.64	92.38	93.4
	X & L & C	95.49	95.68	94.37	93.22		X & L & C	93.15	92.00	92.38	93.04
ResNet 101-v2	X	94.15	95.04	93.37	93.04	NASNet Large	X	94.49	94.08	93.21	92.12
	L	94.82	96.00	93.87	95.42		L	94.82	94.56	94.2	93.58
	C	93.15	94.88	94.37	93.58		C	94.49	93.44	94.37	92.49
	X & L	94.32	95.2	93.54	94.68		X & L	94.65	95.04	93.54	93.40
	X & C	94.49	95.36	93.54	93.04		X & C	93.65	94.40	94.20	92.30
	L & C	94.32	95.36	93.70	95.05		L & C	94.65	94.56	94.20	93.40
	X & L & C	94.15	95.2	93.87	94.13		X & L & C	94.49	94.56	94.03	93.22
ResNet 152-v2	X	93.99	92.48	94.37	93.04	EfficientNet B6	X	84.97	85.92	88.24	88.46
	L	94.65	94.08	94.03	94.13		L	86.47	85.6	88.74	88.64
	C	94.49	93.28	93.21	93.22		C	86.47	85.44	87.91	89.56
	X & L	94.49	94.08	94.03	93.40		X & L	85.14	86.08	88.07	89.01
	X & C	94.49	92.80	93.70	93.40		X & C	85.47	85.44	88.24	89.19
	L & C	94.65	93.76	94.03	94.13		L & C	86.47	86.08	88.90	89.74
	X & L & C	94.82	94.08	94.37	93.95		X & L & C	85.80	85.76	88.41	89.19

Table 5Binary classification **F1-score** results on BreakHis dataset.

Feature extractor	Classifier(s)	Result (F1-Score \times 100)			
		40 \times	100 \times	200 \times	400 \times
VGG 16	X	90.23	87.22	88.45	84.36
	L	90.67	88.17	89.87	85.18
	C	90.97	88.89	90.06	85.50
	X & L	91.48	88.38	89.47	85.68
	X & C	90.99	87.90	89.50	85.38
	L & C	90.91	89.22	89.75	85.93
	X & L & C	91.28	88.45	89.52	85.42
VGG 19	X	90.23	86.50	88.27	84.47
	L	89.70	88.38	88.76	85.07
	C	90.71	88.29	89.93	86.04
	X & L	90.44	87.46	89.86	86.41
	X & C	91.11	87.62	89.94	86.23
	L & C	90.14	88.17	89.35	86.11
	X & L & C	90.52	87.99	90.24	86.19
ResNet 50	X	91.70	92.55	93.16	93.10
	L	92.98	92.77	93.35	92.78
	C	92.54	92.94	93.62	92.62
	X & L	92.96	93.24	93.60	92.87
	X & C	92.68	93.27	93.85	92.89
	L & C	93.21	92.94	93.49	93.28
	X & L & C	92.77	93.39	93.73	93.28
ResNet 101	X	90.49	90.44	91.04	90.69
	L	90.64	91.61	92.34	91.25
	C	91.14	91.47	92.92	92.35
	X & L	90.47	91.30	92.03	90.98
	X & C	91.03	91.56	92.56	91.50
	L & C	91.26	91.94	92.65	91.79
	X & L & C	90.80	91.77	92.54	91.52
ResNet 152	X	90.54	89.41	91.83	89.82
	L	90.43	90.00	91.93	90.07
	C	90.62	90.93	92.02	89.22
	X & L	90.70	89.97	92.65	89.82
	X & C	91.08	90.40	92.15	90.19
	L & C	90.66	90.11	92.52	90.00
	X & L & C	90.74	90.11	92.25	90.51
ResNet 50-v2	X	96.83	95.90	95.34	94.54
	L	96.24	96.80	95.84	95.60
	C	96.27	96.82	95.50	94.82
	X & L	97.07	97.03	95.95	95.33
	X & C	97.06	96.46	95.71	94.57
	L & C	96.48	96.91	96.08	95.08
	X & L & C	96.84	96.91	95.95	94.94
ResNet 101-v2	X	95.89	96.46	95.25	94.79
	L	96.37	97.15	95.60	96.56
	C	95.20	96.35	95.99	95.20
	X & L	96.02	96.57	95.34	96.03
	X & C	96.12	96.69	95.40	94.79
	L & C	96.02	96.69	95.49	96.29
	X & L & C	95.90	96.58	95.60	95.62
ResNet 152-v2	X	95.77	94.67	95.96	94.77
	L	96.24	95.81	95.77	95.60
	C	96.13	95.23	95.12	94.92
	X & L	96.12	95.81	95.75	95.04
	X & C	96.12	94.90	95.49	95.04
	L & C	96.24	95.58	95.75	95.60
	X & L & C	96.35	95.80	95.99	95.47
Inception v3	X	96.13	95.51	96.21	95.21
	L	97.06	96.15	96.10	96.01
	C	96.60	95.41	95.48	95.62
	X & L	96.47	95.72	96.34	96.42
	X & C	96.61	95.60	96.21	96.16
	L & C	96.71	95.83	96.21	96.14
	X & L & C	96.82	95.94	96.09	96.42
Inception ResNet v2	X	97.42	96.69	96.69	96.98
	L	97.75	96.80	97.75	97.24
	C	98.23	97.04	97.28	96.98
	X & L	97.52	97.03	97.64	97.38
	X & C	97.76	97.27	97.41	96.84
	L & C	97.87	97.25	97.64	96.56
	X & L & C	97.76	97.03	97.87	97.11
DenseNet 121	X	95.80	96.58	95.37	96.42
	L	95.92	97.05	96.09	96.41
	C	95.91	96.23	95.60	95.88
	X & L	96.26	97.27	95.96	96.11
	X & C	95.79	96.57	95.70	96.40
	L & C	95.79	96.70	95.98	96.55
	X & L & C	96.25	96.58	96.45	96.39
DenseNet 169	X	96.25	97.16	95.85	95.97
	L	96.24	97.61	95.85	95.28
	C	95.20	97.27	96.32	95.86
	X & L	96.25	97.05	95.85	95.56
	X & C	95.79	96.94	95.84	95.97
	L & C	95.90	97.50	96.19	95.44
	X & L & C	96.03	97.17	96.20	95.45
DenseNet 201	X	95.14	96.58	95.29	96.42
	L	95.79	96.71	96.44	96.14
	C	95.66	96.69	96.09	95.17
	X & L	96.16	96.48	96.21	96.28
	X & C	95.58	96.35	95.86	96.02
	L & C	95.91	96.94	96.32	95.75
	X & L & C	96.04	96.82	96.45	95.88
Xception	X	94.46	93.55	94.84	94.66
	L	95.55	94.31	94.34	95.60
	C	93.72	94.16	94.06	92.99
	X & L	95.53	94.43	95.04	95.07
	X & C	94.74	94.43	94.03	94.15
	L & C	95.07	94.66	94.59	95.08
	X & L & C	95.18	94.20	94.56	94.81
NASNet Large	X	96.15	95.72	95.11	94.05
	L	96.37	96.09	95.81	95.19
	C	96.14	95.32	95.97	94.36
	X & L	96.26	96.44	95.34	95.03
	X & C	95.58	95.99	95.84	94.21
	L & C	96.26	96.10	95.83	95.03
	X & L & C	96.15	96.11	95.71	94.91
EfficientNet B6	X	89.73	90.20	91.70	91.33
	L	90.70	90.07	92.07	91.55
	C	90.83	90.05	91.50	92.29
	X & L	89.85	90.41	91.59	91.87
	X & C	90.10	90.03	91.73	92.02
	L & C	90.74	90.47	92.24	92.39
	X & L & C	90.31	90.25	91.88	91.99

4.4. Discussion

Analysis of breast cancer histopathological images by utilizing image processing methods developed for the medical field has received much attention as of late. Non-automatic examination of breast cancer histopathological images is susceptible to a host of problems including observer variability, human error and an extremely tedious procedure [46]. A solution that alleviates these obstacles is the use of CAD systems. In this study, we proposed a new model for breast cancer histopathology images binary classification based on deep feature transfer learning. In comparing the IRv2-CXL results to other existing binary breast tumour classification methods, the proposed deep feature method attains better or comparable performance without using any image augmentation (see Table 6), signifying transfer learning and GBDT's potential in this task while demonstrating ensemble methods' power in predictive accuracy and bias/variance trade-off. With regards to improved results, we believe that a better CAD system can be developed by using IRv2-CXL as its foundation.

As illustrated in Table 6, IRv2-CXL achieved better results than the 16 models included in the table in three of the four magnification factors. In the 40 \times magnification factor, the proposed model outperformed almost all the other models by a considerable margin, the only close ones being Sharma and Kumar [47] with 96.25% and Kumar et al. [48] with 94.11%. IRv2-CXL attained a 95.84% accuracy in the 100 \times magnification factor, only outdone by the 96.25% achieved by Sharma and Kumar [47] with a 0.41% margin. The 200 \times magnification factor led to the best individual magnification result of the proposed model. In this magnification, IRv2-CXL and the Kumar et al. [48] model surpassed the other models with at best, a 1.27% and worst, an 18.91% accuracy gap by achieving the same 97.01% accuracy. In the 400 \times magnification factor, the proposed model secured the best result by a 2.04% margin with a 96.15% accuracy score; the second-best model being Sharma and Kumar's [47]. On average IRv2-CXL model attained the best accuracy, 96.46%, followed by Sharma and Kumar's [47] model with a 95.58% average accuracy score.

We decided to use GBDT based methods as classifier because of their high prediction accuracy, and adaptability to non-linear characteristics and good training effect [31, 49]. XGBoost, CatBoost and LightGBM were chosen as classifier candidates. XGBoost was chosen because of its new regularization method that resists overfitting, therefore making the model more robust [31, 50]. CatBoost's improved generalization as well as its ability to capture high-order dependencies makes it a viable candidate as well [51]. Last but not least LightGBM is an attractive method to use as a classifier because of its capability in handling large-scale data. In addition, CatBoost's leaf-wise growth approach makes it more accurate than other level-wise GBDT methods [31, 52]. As all three of our classifier candidates performed relatively well on this task, we decided to incorporate a soft majority voting method in the proposed method to enhance its predictive performance and improve the model's robust-

ness by lowering its variance. We found that IRv2-CXL, a model with Inception-ResNet-v2 as its feature extractor and soft majority voting ensemble of XGBoost, CatBoost and LightGBM achieves better magnification-wise average accuracy than other models we experimented on.

IRv2-CXL has several advantages in comparison to other existing models. By using a pre-trained model as feature extractor, its training time is much less than those models that attempt to extract features from images themselves. The use of transfer learning also reduces the proposed model's need for huge amounts of training data which is almost always in short supply in the medical field. Incorporating an ensemble of GBDT based algorithms in the IRv2-CXL classifier not only improves its accuracy in comparison to other models but also draws attention to the fact that not enough scrutiny has been afforded to choosing classifiers in previous studies and most of the researchers tackling this task have focused on developing better feature extractors [53]. The use of soft majority voting provides IRv2-CXL with a lower variance relative to other models. As the proposed model performs well with all magnifications present in BreakHis and has low accuracy variance across all of them, a CAD system based on it would have an extremely low dependency on the magnification factor. While the proposed model has many advantages, it has weaknesses as well. The first weakness stems from a lack of feature extractor fine-tuning. Inception-ResNet-v2's large image data belongs mostly to the general domain, such as ear, corn and vase, however, this task's images are breast cancer histopathology images with non-identical visual appearances which may make IRv2-CXL's feature extractor biased with the source data and less generalized on the target data [54]. The second weakness arises from the dataset we used to develop this model and the blatant imbalance in its class distributions. While our model performs well on the F1 score (Table 3) and ROC curve (Figure 6) as well as accuracy and its high accuracy is not reliant on this imbalance, we believe a more balanced dataset would produce even better results.

In the future, we aim to resolve the proposed model's lack of generalization on the target dataset through fine-tuning and addressing the imbalanced dataset issue with a more comprehensive preprocessing including an image augmentation that makes the model more balanced. Further improvements can be achieved by incorporating pathologist expertise and the grad-cam images we have already produced. These two can help us determine the nonconformities between the areas that help the expert and IRv2-CXL decide on tumour classification, then we can construct an attention-based model targeting those areas most helpful to correct classification.

Table 6

Comparison of IRv2-CXL with other models.

Study (Year)	Results (Accuracy %)				
	40×	100×	200×	400×	Average
Spanhol et al. [55] (2017)	84.60	84.80	84.20	81.60	83.80
Song et al. [56] (2017)	87.00	86.20	85.20	82.90	85.32
Song et al. [57] (2017)	87.70	87.60	86.50	83.90	86.42
Alirezazadeh et al. [8] (2018)	89.10	87.30	91.00	86.60	88.50
Sanchez et al. [58] (2018)	85.90	80.40	78.10	71.10	78.87
Benhammou et al. [59] (2018)	85.50	83.20	85.40	80.30	83.60
Du et al. [60] (2018)	90.69	90.46	90.64	90.96	90.68
Badejo et al. [61] (2018)	91.10	90.70	86.20	84.30	88.07
Nahid et al. [62] (2018)	88.70	85.30	88.60	88.40	87.75
Kumar and Rao [63] (2018)	82.00	86.20	84.60	84.00	84.20
Sudharshan et al. [64] (2019)	87.80	85.60	80.80	82.90	84.27
Kumar et al. [48] (2020)	94.11	95.12	97.01	93.40	94.91
Li et al. [65] (2021)	87.85	86.68	87.75	85.30	86.89
Sharma and Kumar [47] (2022)	96.25	96.25	95.74	94.11	95.58
Joseph et al. [66] (2022)	90.87	89.57	91.58	88.67	90.17
Zerouaoui and Idri [67] (2022)	92.61	92.00	93.93	91.73	92.56
IRv2-CXL (2022)	96.82	95.84	97.01	96.15	96.46

5. Conclusion

In this paper, we tackled the issue of breast tumour type (benign or malignant) estimation by processing histopathological images obtained from the lab. This tumour type assessment remains an unsolved problem in early cancer detection that by resolving it with the help of an automatic classification system we can contribute greatly to the medical community and ordinary people, saving them money, time and above all lives.

IRv2-CXL, a novel binary classification method for CAD systems is introduced in this work. Most CAD systems consist of three phases, we chose to concentrate on the classification phase. This approach implements deep features extracted from a pre-trained network and a classifier to distinguish between benign and malignant tumours. 16 different pre-trained networks were tested with seven classifiers (three single and four ensembles). The best model was found to be an Inception-ResNet-v2 network and a soft majority voting ensemble of gradients boosted decision trees (i.e., CatBoost,...) named IRv2-CXL. IRv2-CXL was trained on and then validated using the BreakHis dataset. IRv2-CXL achieved an accuracy of 96.83%, 95.84%, 97.02%, and 96.16% on the 40×, 100×, 200×, and 400× magnification factors, respectively. Furthermore, a class activation mapping was also implemented to identify important regions in the image that help IRv2-CXL classify tumours to make sure the proposed model is not concentrating on any unrelated parts.

We believe that further improvements to this model or the ideas it is based on are entirely possible and within reach. We hope that this study will attract others to explore the ideas presented and build upon our and other existing research findings to introduce even better methods with more outstanding results.

6. Data and Code Availability

The BreakHis dataset (version 1) is publicly available [here](#). In addition, the source code of the proposed model required to reproduce the predictions and results is available at the public [Github repository](#).

7. Declaration of Competing Interest

The authors express that they have no competing interest affecting the reported work in this article.

References

- [1] Mohamed Abdul-Al, Amir Zaernia, and Farshid Sefat. Biomaterials for breast reconstruction: Promises, advances, and challenges. *Journal of Tissue Engineering and Regenerative Medicine*, 14(11):1549–1569, 2020.
- [2] Victoria Harmer. Breast cancer. part 1: Awareness and common benign diseases. *British Journal of Nursing*, 17(15):950–955, 2008.
- [3] Hamideh Hajiabadi, Vahide Babaiyan, Davood Zabihzadeh, and Moein Hajiabadi. Combination of loss functions for robust breast cancer prediction. *Computers & Electrical Engineering*, 84:106624, 2020.
- [4] Mazin Abed Mohammed, Belal Al-Khateeb, Ahmed Noori Rashid, Dheyaa Ahmed Ibrahim, Mohd Khanapi Abd Ghani, and Salama A Mostafa. Neural network and multi-fractal dimension features for breast cancer classification from ultrasound images. *Computers & Electrical Engineering*, 70:871–882, 2018.
- [5] Faezehsadat Shahidi, Salwani Mohd Daud, Hafiza Abas, Noor Azurati Ahmad, and Nurazeen Maarop. Breast cancer classification using deep learning approaches and histopathology image: a comparison study. *IEEE Access*, 8:187531–187552, 2020.
- [6] Saad Awadh Alanazi, MM Kamruzzaman, Md Nazirul Islam Sarker, Madallah Alruwaili, Yousef Alhwaiti, Nasser Alshammari, and Muhammad Hameed Siddiqi. Boosting breast cancer detection using convolutional neural network. *Journal of Healthcare Engineering*, 2021, 2021.
- [7] S Punitha, Fadi Al-Turjman, and Thompson Stephan. An automated breast cancer diagnosis using feature selection and parameter opti-

- mization in ann. *Computers & Electrical Engineering*, 90:106958, 2021.
- [8] Pendar Alirezazadeh, Behzad Hejrati, Alireza Monsef-Esfahani, and Abdolhossein Fathi. Representation learning-based unsupervised domain adaptation for classification of breast cancer histopathology images. *Biocybernetics and Biomedical Engineering*, 38(3):671–683, 2018.
- [9] Claudia Perlich, Brian Dalessandro, Troy Raeder, Ori Stitelman, and Foster Provost. Machine learning for targeted display advertising: Transfer learning in action. *Machine learning*, 95(1):103–127, 2014.
- [10] Yizhi Lv, Jianing Xue, Feng Duan, Zhe Sun, and Junhua Li. An exploratory study of transfer learning frameworks in the context of few available shots of neurophysiological signals. *Computers and Electrical Engineering*, 101:108091, 2022.
- [11] Sakshi Ahuja, Bijaya Ketan Panigrahi, Nilanjan Dey, Venkatesan Rajinikanth, and Tapan Kumar Gandhi. Deep transfer learning-based automated detection of covid-19 from lung ct scan slices. *Applied Intelligence*, 51(1):571–585, 2021.
- [12] Shahid Munir Shah, Rizwan Ahmed Khan, Sheeraz Arif, and Unaiza Sajid. Artificial intelligence for breast cancer analysis: Trends & directions. *Computers in Biology and Medicine*, page 105221, 2022.
- [13] Irene Fondón, Auxiliadora Sarmiento, Ana Isabel García, María Silvestre, Catarina Eloy, António Polónia, and Paulo Aguiar. Automatic classification of tissue malignancy for breast carcinoma diagnosis. *Computers in biology and medicine*, 96:41–51, 2018.
- [14] Kalpana George, Shameer Faziludeen, Praveen Sankaran, et al. Breast cancer detection from biopsy images using nucleus guided transfer learning and belief based fusion. *Computers in Biology and Medicine*, 124:103954, 2020.
- [15] Fabio A Spanhol, Luiz S Oliveira, Caroline Petitjean, and Laurent Heutte. A dataset for breast cancer histopathological image classification. *Ieee transactions on biomedical engineering*, 63(7):1455–1462, 2015.
- [16] Marc Macenko, Marc Niethammer, James S Marron, David Borland, John T Woosley, Xiaojun Guan, Charles Schmitt, and Nancy E Thomas. A method for normalizing histology slides for quantitative analysis. In *2009 IEEE international symposium on biomedical imaging: from nano to macro*, pages 1107–1110. IEEE, 2009.
- [17] Tejalal Choudhary, Vipul Mishra, Anurag Goswami, and Jagannathan Sarangapani. A transfer learning with structured filter pruning approach for improved breast cancer classification on point-of-care devices. *Computers in Biology and Medicine*, 134:104432, 2021.
- [18] Nusrat Ameen Barsha, Aimon Rahman, and MRC Mahdy. Automated detection and grading of invasive ductal carcinoma breast cancer using ensemble of deep learning models. *Computers in Biology and Medicine*, 139:104931, 2021.
- [19] Caroline Barcelos Gonçalves, Jefferson R de Souza, and Henrique Fernandes. Cnn architecture optimization using bio-inspired algorithms for breast cancer detection in infrared images. *Computers in Biology and Medicine*, page 105205, 2022.
- [20] Somnath Chatterjee, Shreya Biswas, Arindam Majee, Shibaprasad Sen, Diego Oliva, and Ram Sarkar. Breast cancer detection from thermal images using a grunwald-letnikov-aided dragonfly algorithm-based deep feature selection method. *Computers in biology and medicine*, 141:105027, 2022.
- [21] Stevo Bozinovski. Reminder of the first paper on transfer learning in neural networks, 1976. *Informatica*, 44(3), 2020.
- [22] Jia Deng, Wei Dong, Richard Socher, Li-Jia Li, Kai Li, and Li Fei-Fei. Imagenet: A large-scale hierarchical image database. In *2009 IEEE conference on computer vision and pattern recognition*, pages 248–255. Ieee, 2009.
- [23] Christian Szegedy, Sergey Ioffe, Vincent Vanhoucke, and Alexander A Alemi. Inception-v4, inception-resnet and the impact of residual connections on learning. In *Thirty-first AAAI conference on artificial intelligence*, 2017.
- [24] Ramprasaath R Selvaraju, Michael Cogswell, Abhishek Das, Ramakrishna Vedantam, Devi Parikh, and Dhruv Batra. Grad-cam: Visual explanations from deep networks via gradient-based localization. In *Proceedings of the IEEE international conference on computer vision*, pages 618–626, 2017.
- [25] Jaehoon Kim, Jeongkyu Oh, and Tae-Young Heo. Acoustic scene classification and visualization of beehive sounds using machine learning algorithms and grad-cam. *Mathematical Problems in Engineering*, 2021, 2021.
- [26] Nianwen Si, Wenlin Zhang, Dan Qu, Xiangyang Luo, Heyu Chang, and Tong Niu. Spatial-channel attention-based class activation mapping for interpreting cnn-based image classification models. *Security and Communication Networks*, 2021, 2021.
- [27] Peizhen Xie, Ke Zuo, Jie Liu, Mingliang Chen, Shuang Zhao, Wenjie Kang, and Fangfang Li. Interpretable diagnosis for whole-slide melanoma histology images using convolutional neural network. *Journal of healthcare engineering*, 2021, 2021.
- [28] Hamid Nasiri and Seyed Ali Alavi. A Novel Framework Based on Deep Learning and ANOVA Feature Selection Method for Diagnosis of COVID-19 Cases from Chest X-Ray Images. *Computational Intelligence and Neuroscience*, 2022:4694567, 2022.
- [29] Hamid Nasiri and Sharif Hasani. Automated detection of COVID-19 cases from chest X-ray images using deep neural network and XGBoost. *Radiography*, 28(3):732–738, 2022.
- [30] Eali Stephen Neal Joshua, Debnath Bhattacharyya, Midhun Chakkravarthy, and Yung-Cheol Byun. 3d cnn with visual insights for early detection of lung cancer using gradient-weighted class activation. *Journal of Healthcare Engineering*, 2021, 2021.
- [31] Yanwei Xu, Weiwei Cai, Liuyang Wang, and Tancheng Xie. Intelligent diagnosis of rolling bearing fault based on improved convolutional neural network and lightgbm. *Shock and Vibration*, 2021, 2021.
- [32] Nidhi Kalidas Sawant, Shivnarayan Patidar, Naimahmed Nesaragi, and U Rajendra Acharya. Automated detection of abnormal heart sound signals using fano-factor constrained tunable quality wavelet transform. *Biocybernetics and Biomedical Engineering*, 41(1):111–126, 2021.
- [33] Hamid Nasiri, Ghazal Kheyroddin, Morteza Dorrigiv, Mona Esmaeili, Amir Raeisi Nafchi, Mohsen Haji Ghorbani, and Payman Zarkesh-Ha. Classification of COVID-19 in Chest X-ray Images Using Fusion of Deep Features and LightGBM. In *2022 IEEE World AI IoT Congress (AIIoT)*, pages 201–206, 2022.
- [34] Mobina Ezzoddin, Hamid Nasiri, and Morteza Dorrigiv. Diagnosis of covid-19 cases from chest x-ray images using deep neural network and lightgbm. In *2022 International Conference on Machine Vision and Image Processing (MVIP)*, pages 1–7. IEEE, 2022.
- [35] Fangrong Zhou, Hao Pan, Zhenyu Gao, Xuyong Huang, Guochao Qian, Yu Zhu, and Feng Xiao. Fire prediction based on catboost algorithm. *Mathematical Problems in Engineering*, 2021, 2021.
- [36] Essam Al Daoud. Comparison between xgboost, lightgbm and catboost using a home credit dataset. *International Journal of Computer and Information Engineering*, 13(1):6–10, 2019.
- [37] Xiao-yi Wang, Yi Yang, Yu-ting Bai, Jia-bin Yu, Zhi-yao Zhao, and Xue-bo Jin. Fuzzy boost classifier of decision experts for multicriteria group decision-making. *Complexity*, 2020, 2020.
- [38] Tianqi Chen and Carlos Guestrin. Xgboost: A scalable tree boosting system. In *Proceedings of the 22nd acm sigkdd international conference on knowledge discovery and data mining*, pages 785–794, 2016.
- [39] Saeed Chehreh Chelgani, Hamid Nasiri, and Mehdi Alidokht. Interpretable modeling of metallurgical responses for an industrial coal column flotation circuit by xgboost and shap-a “conscious-lab” development. *International Journal of Mining Science and Technology*, 31(6):1135–1144, 2021.
- [40] Saeed Chehreh Chelgani, Hamid Nasiri, and Arash Tohy. Modeling of particle sizes for industrial hpg products by a unique explainable ai tool-a “conscious lab” development. *Advanced Powder Technology*, 32(11):4141–4148, 2021.
- [41] Zeinab Akhavan, Mona Esmaeili, Dimitrios Sikeridis, and Michael Devetsikiotis. Internet of Things-enabled passive contact tracing in smart cities. *Internet of Things*, page 100397, 2021.
- [42] Hamid Nasiri, Arman Homafar, and Saeed Chehreh Chelgani. Prediction of uniaxial compressive strength and modulus of elasticity for

- travertine samples using an explainable artificial intelligence. *Results in Geophysical Sciences*, 8:100034, 2021.
- [43] Sharif Hasani and Hamid Nasiri. COV-ADSOX: An Automated Detection System using X-ray images, deep learning, and XGBoost for COVID-19. *Software Impacts*, 11:100210, 2022.
- [44] Deepak Gupta and Rinkle Rani. Improving malware detection using big data and ensemble learning. *Computers & Electrical Engineering*, 86:106729, 2020.
- [45] Yassir Benhammou, Boujemaa Achchab, Francisco Herrera, and Siham Tabik. Breakhis based breast cancer automatic diagnosis using deep learning: Taxonomy, survey and insights. *Neurocomputing*, 375:9–24, 2020.
- [46] R Rashmi, Keerthana Prasad, and Chethana Babu K Udupa. Breast histopathological image analysis using image processing techniques for diagnostic puposes: A methodological review. *Journal of Medical Systems*, 46(1):1–24, 2022.
- [47] Shalu Sharma and Sumit Kumar. The xception model: A potential feature extractor in breast cancer histology images classification. *ICT Express*, 8(1):101–108, 2022.
- [48] Abhinav Kumar, Sanjay Kumar Singh, Sonal Saxena, K Lakshmanan, Arun Kumar Sangaiah, Himanshu Chauhan, Sameer Shrivastava, and Raj Kumar Singh. Deep feature learning for histopathological image classification of canine mammary tumors and human breast cancer. *Information Sciences*, 508:405–421, 2020.
- [49] Weigang Wang, Tao Li, Wenrui Wang, and Zhenzhen Tu. Multiple fingerprints-based indoor localization via gbd: Subspace and rssi. *IEEE Access*, 7:80519–80529, 2019.
- [50] Rasoul Fatahi, Hamid Nasiri, Ehsan Dadfar, and Saeed Chehreh Chelgani. Modeling of energy consumption factors for an industrial cement vertical roller mill by SHAP-XGBoost: a "conscious lab" approach. *Scientific Reports*, 12(1):1–13, 2022.
- [51] Mei Zhang, Wanli Chen, Yu Zhang, Fei Liu, Dongshun Yu, Chaoyin Zhang, and Li Gao. Fault diagnosis of oil-immersed power transformer based on difference-mutation brain storm optimized catboost model. *IEEE Access*, 9:168767–168782, 2021.
- [52] Ying Zhang, Yanhao Wang, Minghe Gao, Qunfei Ma, Jing Zhao, Rongrong Zhang, Qingqing Wang, and Linyan Huang. A predictive data feature exploration-based air quality prediction approach. *IEEE Access*, 7:30732–30743, 2019.
- [53] Alan Chan and Jack A Tuszyński. Automatic prediction of tumour malignancy in breast cancer with fractal dimension. *Royal Society open science*, 3(12):160558, 2016.
- [54] Ahmad Shalbaf, Majid Vafaezadeh, et al. Automated detection of covid-19 using ensemble of transfer learning with deep convolutional neural network based on ct scans. *International journal of computer assisted radiology and surgery*, 16(1):115–123, 2021.
- [55] Fabio A Spanhol, Luiz S Oliveira, Paulo R Cavalin, Caroline Petitjean, and Laurent Heutte. Deep features for breast cancer histopathological image classification. In *2017 IEEE International Conference on Systems, Man, and Cybernetics (SMC)*, pages 1868–1873. IEEE, 2017.
- [56] Yang Song, Ju Jia Zou, Hang Chang, and Weidong Cai. Adapting fisher vectors for histopathology image classification. In *2017 IEEE 14th International Symposium on Biomedical Imaging (ISBI 2017)*, pages 600–603. IEEE, 2017.
- [57] Yang Song, Hang Chang, Heng Huang, and Weidong Cai. Supervised intra-embedding of fisher vectors for histopathology image classification. In *International Conference on Medical Image Computing and Computer-Assisted Intervention*, pages 99–106. Springer, 2017.
- [58] Daniel Sanchez-Morillo, Jesús González, Marcial García-Rojo, and Julio Ortega. Classification of breast cancer histopathological images using kaze features. In *International Conference on Bioinformatics and Biomedical Engineering*, pages 276–286. Springer, 2018.
- [59] Yassir Benhammou, Siham Tabik, Boujemaa Achchab, and Francisco Herrera. A first study exploring the performance of the state-of-the-art cnn model in the problem of breast cancer. In *Proceedings of the International Conference on Learning and Optimization Algorithms: Theory and Applications*, pages 1–6, 2018.
- [60] Baolin Du, Qi Qi, Han Zheng, Yue Huang, and Xinghao Ding. Breast cancer histopathological image classification via deep active learning and confidence boosting. In *International Conference on Artificial Neural Networks*, pages 109–116. Springer, 2018.
- [61] Joke A Badejo, Emmanuel Adetiba, Adekunle Akinrinmade, and Matthew B Akanle. Medical image classification with hand-designed or machine-designed texture descriptors: a performance evaluation. In *International Conference on Bioinformatics and Biomedical Engineering*, pages 266–275. Springer, 2018.
- [62] Abdullah-Al Nahid, Aaron Mikaelian, and Yinan Kong. Histopathological breast-image classification with restricted boltzmann machine along with backpropagation. *Biomedical Research*, 29(10):2068–2077, 2018.
- [63] Kundan Kumar and Annavarapu Chandra Sekhara Rao. Breast cancer classification of image using convolutional neural network. In *2018 4th International Conference on Recent Advances in Information Technology (RAIT)*, pages 1–6. IEEE, 2018.
- [64] PJ Sudharshan, Caroline Petitjean, Fabio Spanhol, Luiz Eduardo Oliveira, Laurent Heutte, and Paul Honeine. Multiple instance learning for histopathological breast cancer image classification. *Expert Systems with Applications*, 117:103–111, 2019.
- [65] Xin Li, HongBo Li, WenSheng Cui, ZhaoHui Cai, and MeiJuan Jia. Classification on digital pathological images of breast cancer based on deep features of different levels. *Mathematical Problems in Engineering*, 2021, 2021.
- [66] Agaba Ameh Joseph, Mohammed Abdullahi, Sahalu Balarabe Junaidu, Hayatu Hassan Ibrahim, and Haruna Chiroma. Improved multi-classification of breast cancer histopathological images using hand-crafted features and deep neural network (dense layer). *Intelligent Systems with Applications*, 14:200066, 2022.
- [67] Hasnae Zerouaoui and Ali Idri. Deep hybrid architectures for binary classification of medical breast cancer images. *Biomedical Signal Processing and Control*, 71:103226, 2022.